Lignin-based Non-Isocyanate Polyurethanes by transurethanisation: catalyst selection towards Covalent Adaptable Networks

Aline Rebejac,[1,2] Nathan Wybo,[1] Luc Avérous,[1,*] Antoine Duval[1,2,*]

[1] BioTeam/ICPEES-ECPM, UMR CNRS 7515, Université de Strasbourg, 25 rue Becquerel, 67087 Strasbourg Cedex 2, France

[2] Soprema, 15 rue de Saint Nazaire, 67100 Strasbourg, France

* Corresponding authors: luc.averous@unistra.fr, antoine.duval@unistra.fr

SUPPLEMENTARY INFORMATION

Screening of catalysts for transurethanisation

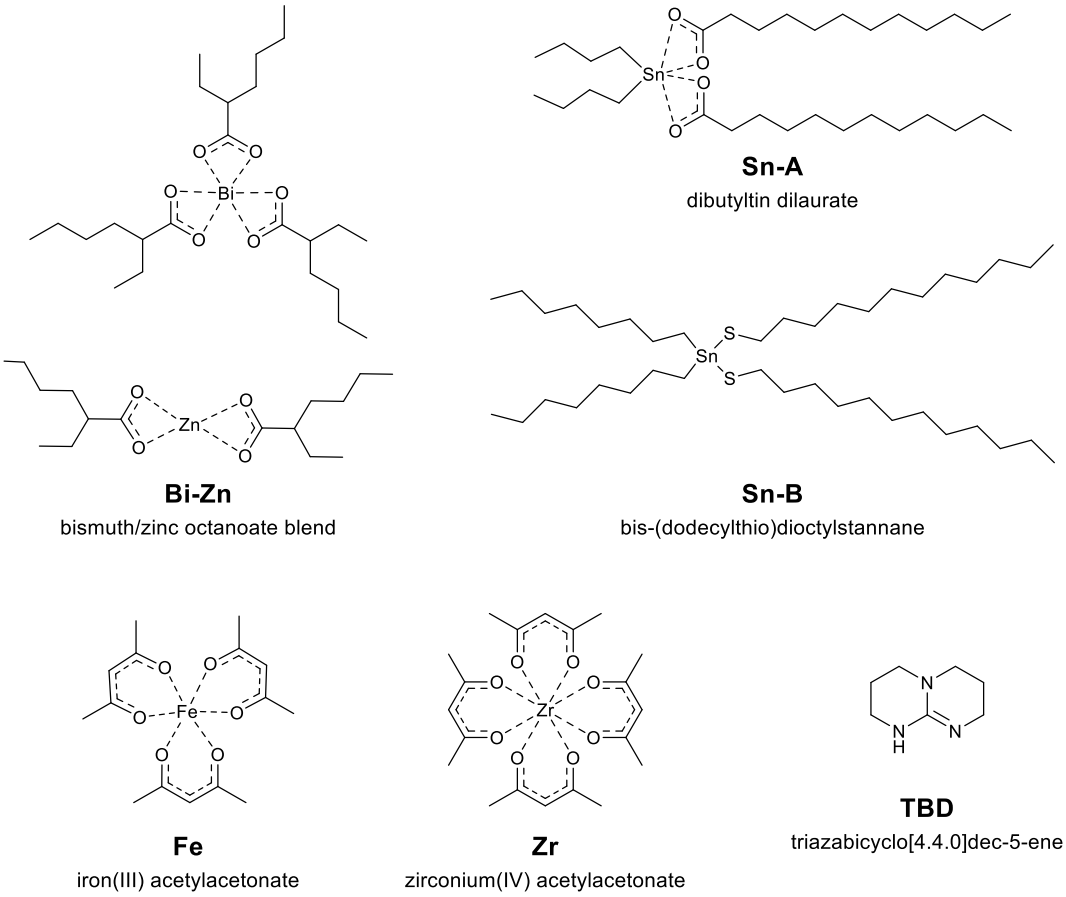

Figure S 1. Structures of the catalysts used in this study.

The yield of urethane product was calculated from the integrations of signals **c** (4H in HMDC and urethane product) and **g** (4H in urethane product) (Figure S 2 to Figure S 9), according to Equation S1:

$$Yield\ urethane\ product\ (\%) = 100\ \times \frac{\int \boldsymbol{g}}{\int \boldsymbol{c}} \qquad \text{(S1)}$$

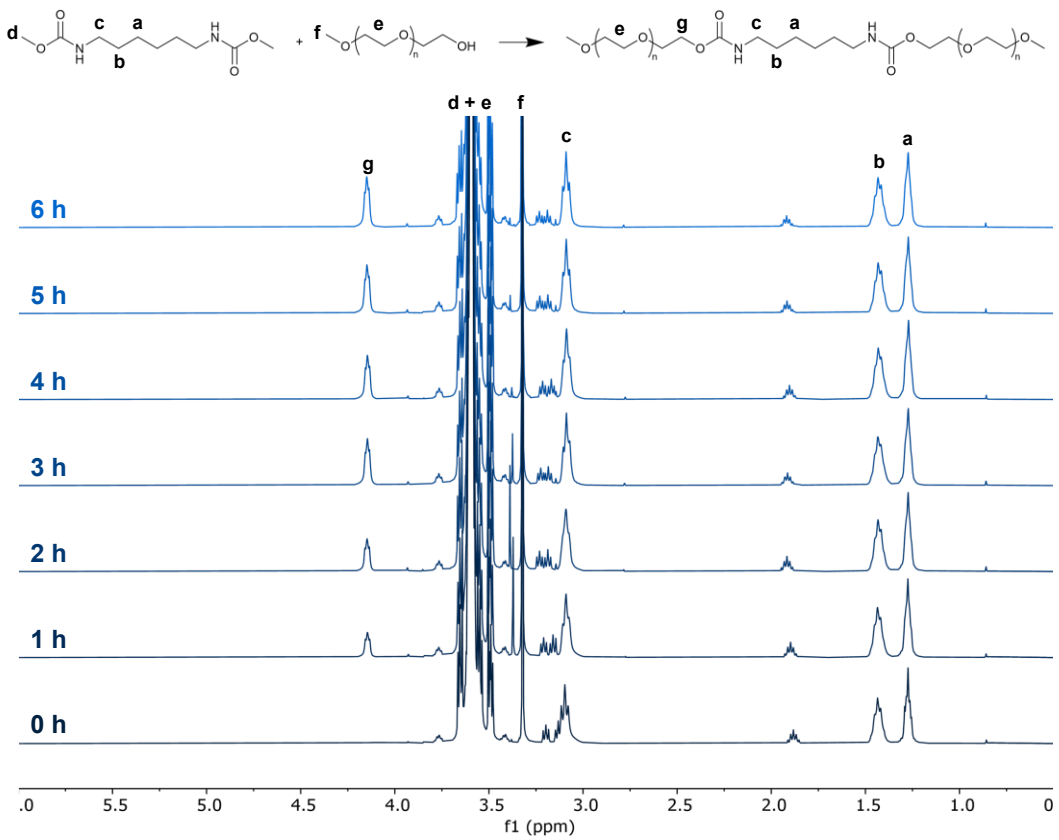

*Figure S 2. ^{1}H NMR spectra (400 MHz, $CDCl_3$) of the model transurethanisation reaction catalysed by **TBD**.*

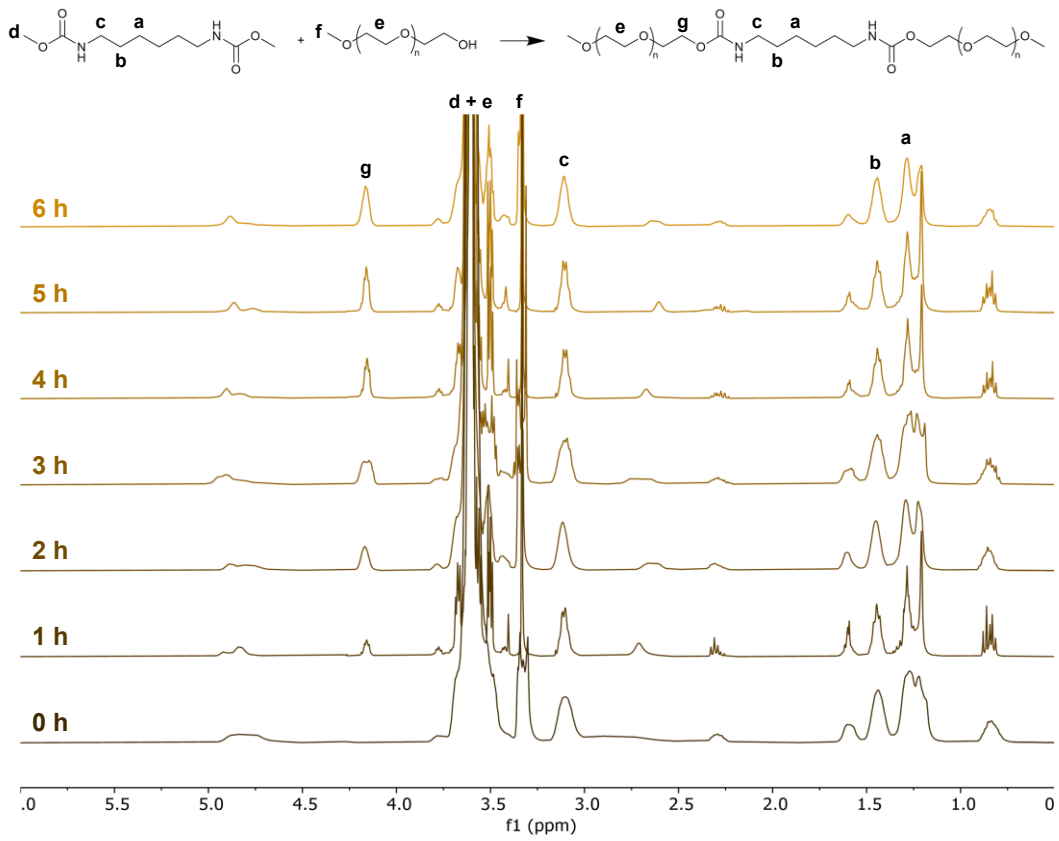

*Figure S 3. ^{1}H NMR spectra (400 MHz, $CDCl_3$) of the model transurethanisation reaction catalysed by **Sn-A**.*

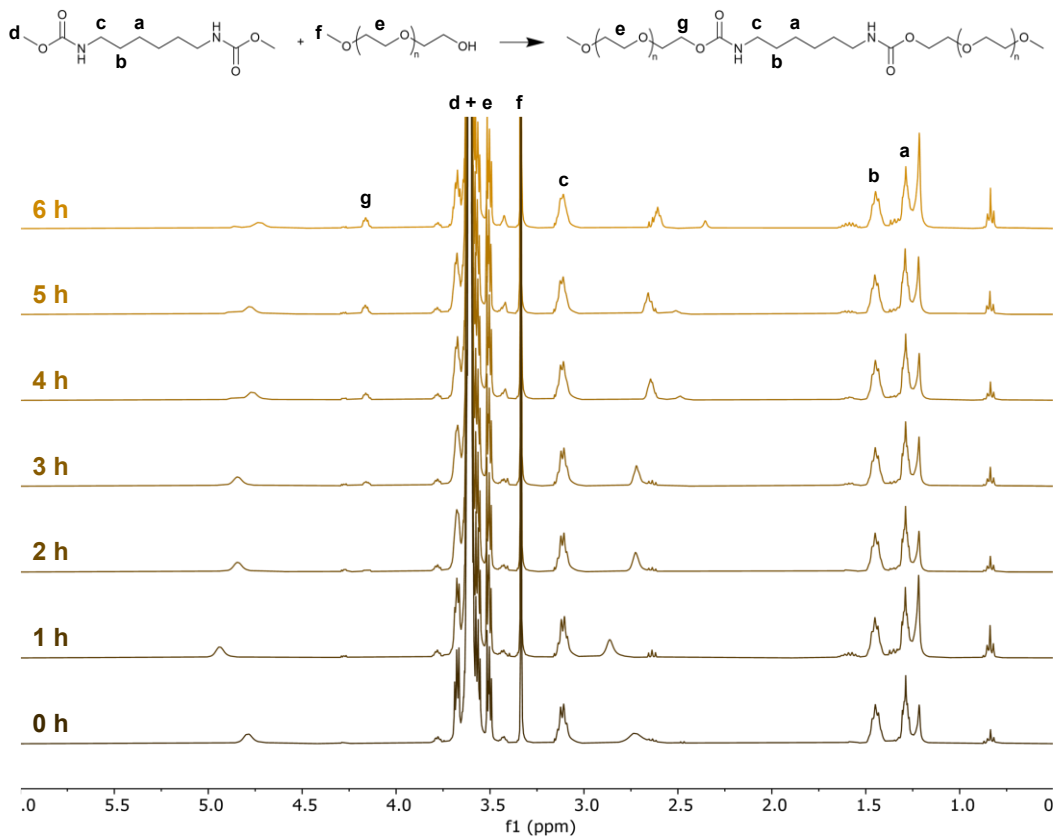

*Figure S 4. ^{1}H NMR spectra (400 MHz, $CDCl_3$) of the model transurethanisation reaction catalysed by **Sn-B**.*

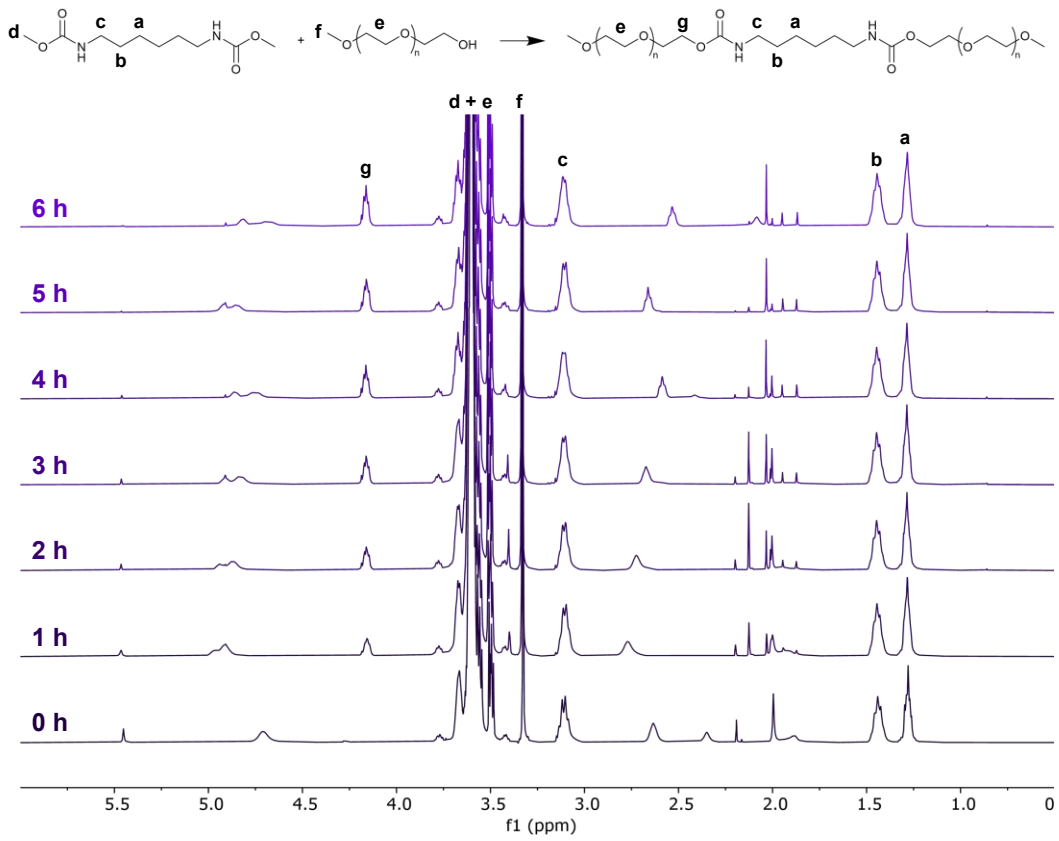

*Figure S 5. ^{1}H NMR spectra (400 MHz, $CDCl_3$) of the model transurethanisation reaction catalysed by **Zr**.*

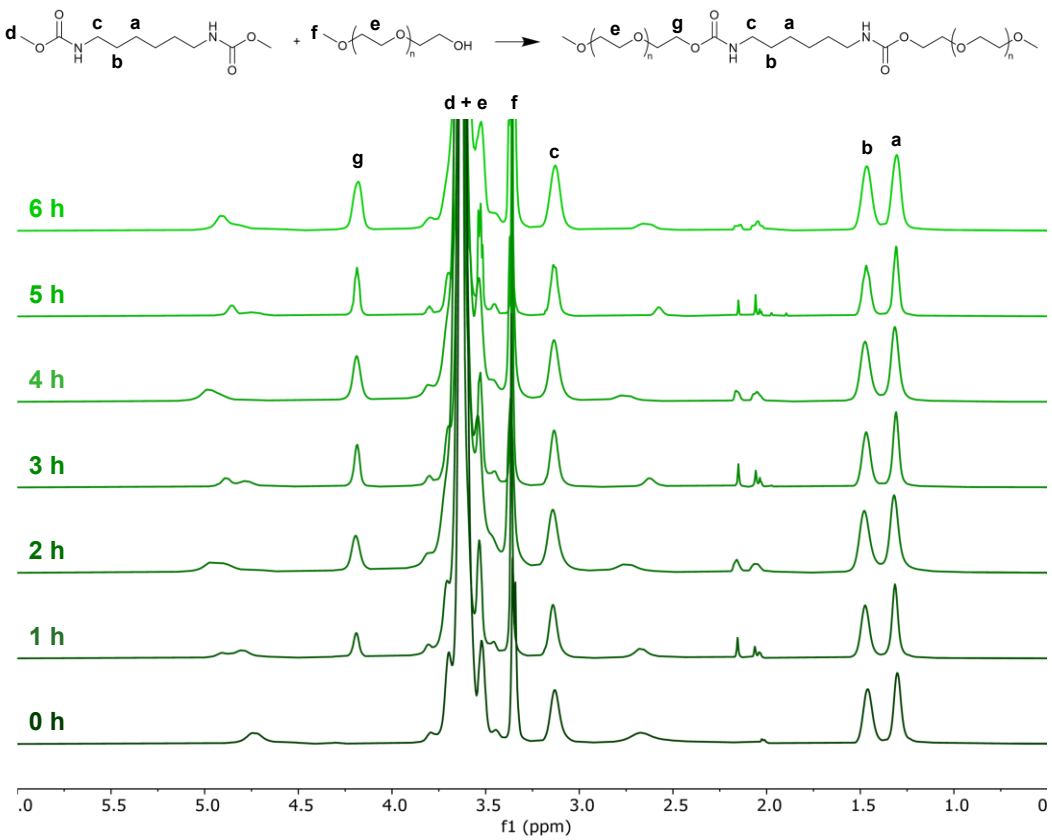

Figure S 6. ^{1}H NMR spectra (400 MHz, $CDCl_3$) of the model transurethanisation reaction catalysed by ***Fe***

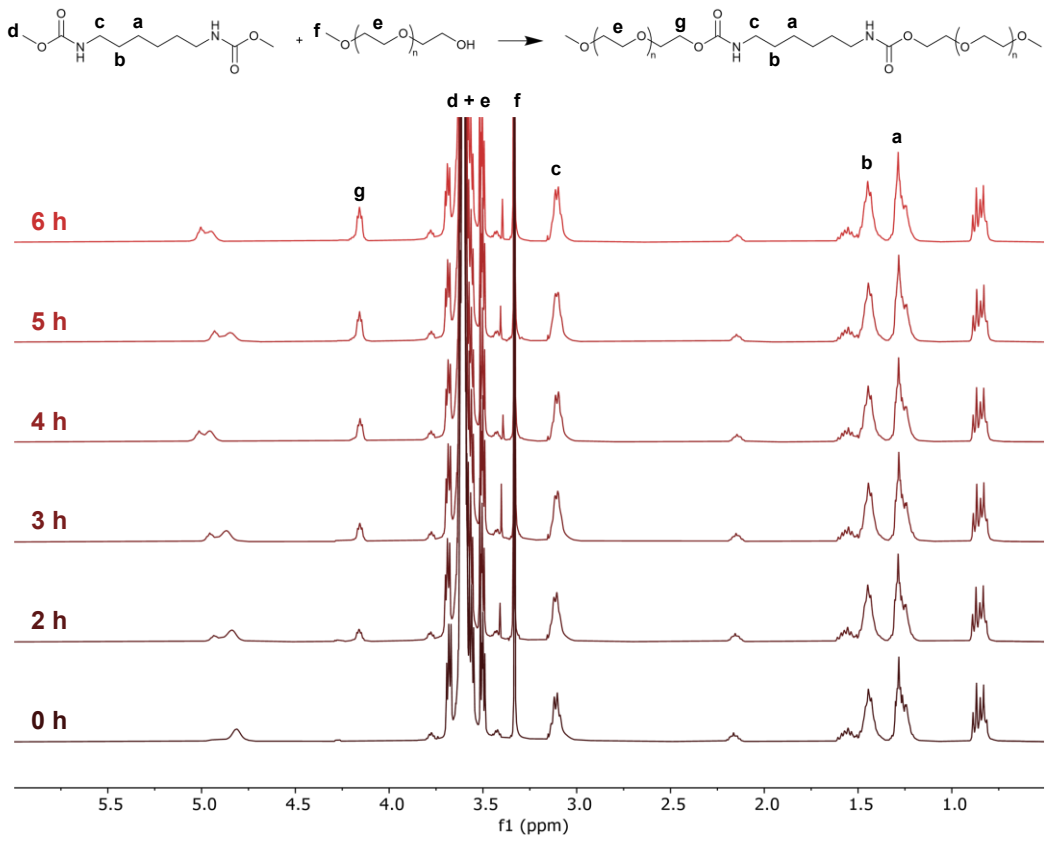

Figure S 7. ^{1}H NMR spectra (400 MHz, $CDCl_3$) of the model transurethanisation reaction catalysed by ***Bi-Zn***.

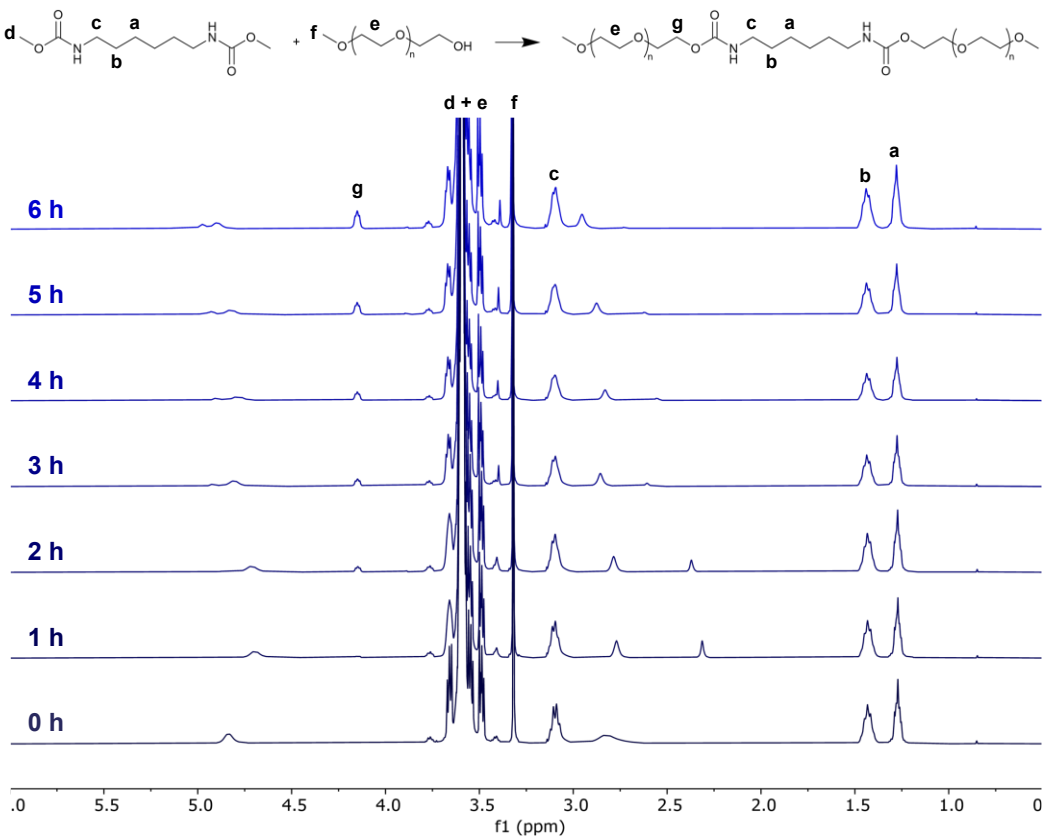

Figure S 8. ^1H NMR spectra (400 MHz, $CDCl_3$) of the model transurethanisation reaction catalysed by ***K_2CO_3***.

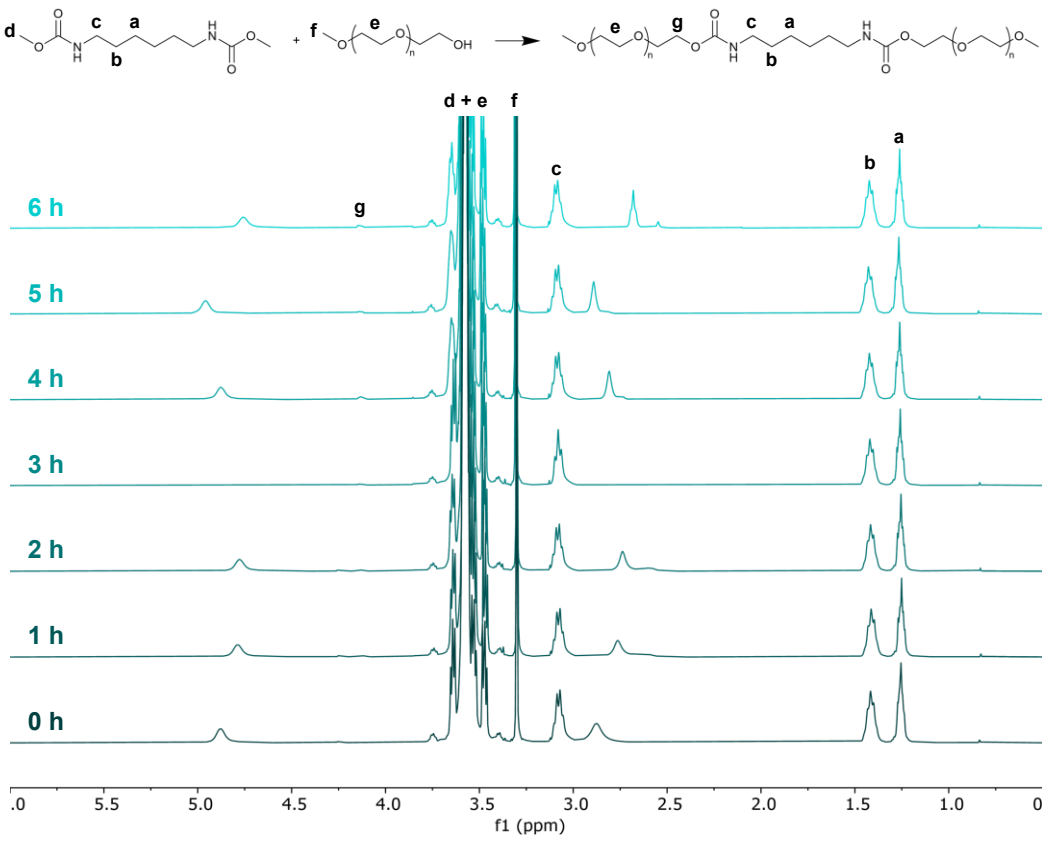

Figure S 9. ^1H NMR spectra (400 MHz, $CDCl_3$) of the model transurethanisation reaction catalysed by ***NaOH***.

The TU reaction was assumed to be first order with respect to both the carbamate and alcohol:[1,2]

$$-\frac{d[HMDC]}{dt} = k\,[HMDC]\,[PEG500MM]$$

Since [PEG500MM] = 2 [HMDC]:

$$-\frac{d[HMDC]}{dt} = 2k\,[HMDC]^2 \;\Leftrightarrow\; -\frac{d[HMDC]}{[HMDC]^2} = 2k\,dt$$

Upon integration, we obtain:

$$\frac{1}{[HMDC]} = 2kt + \frac{1}{[HMDC]_0}$$

Therefore, a plot of 1/[HMDC] = f(t) gives a linear regression of slope 2k (Figure S 10).

$$[HMDC]_0 = \frac{n(HMDC)_0}{V_{tot}}$$

with V_{tot} the total volume of solution. V_{tot} was estimated assuming that the reaction mixture had the density of PEG (1.13 g cm^{-3}).

$$V_{tot} = \frac{m(HMDC) + m(PEG500MM)}{1.13} = \frac{1 + 4.3}{1.13} = 4.69\ cm^3 = 4.69\ 10^{-3}\ L$$

$$[HMDC]_0 = \frac{n(HMDC)_0}{V_{tot}} = \frac{4.3}{4.69} = 0.92\ mol\ L^{-1}$$

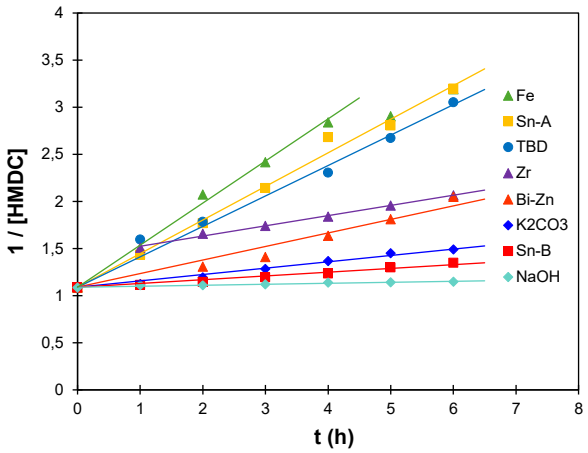

Figure S 10. Plots of 1/[HMDC] = f(t) used to evaluate the reaction rate.

Characterization of lignin-based polyol

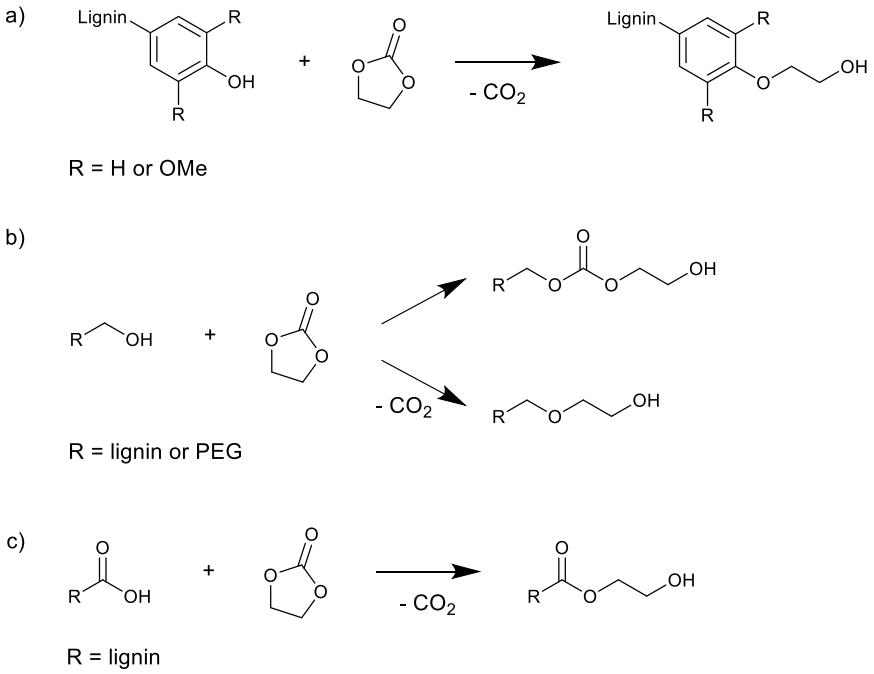

Scheme S 1. Reactions of lignin and PEG during polyol synthesis with EC: (a) reaction of phenolic OH, (b) reaction of aliphatic OH and (c) reaction of COOH. Adapted from Duval et al.[3]

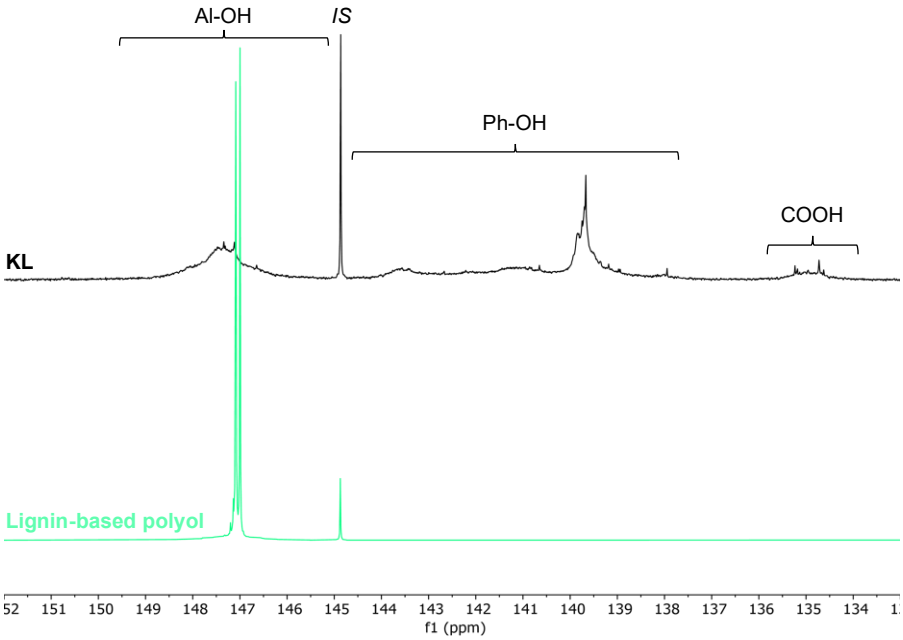

Figure S 11. ^{31}P NMR of KL and the lignin-based polyol synthesized thereof. IS = internal standard.

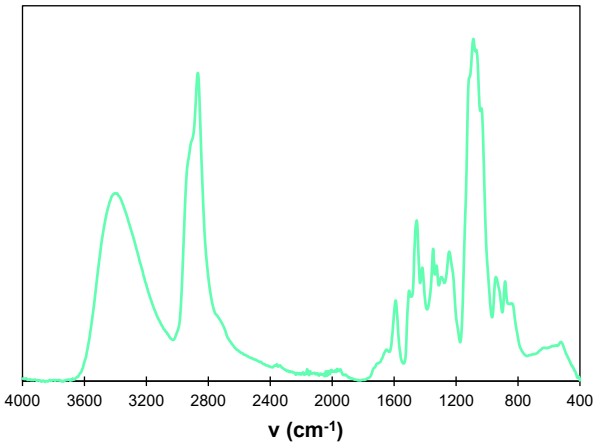

Figure S 12. FTIR spectrum of the lignin-based polyol.

Characterization of NIPU materials

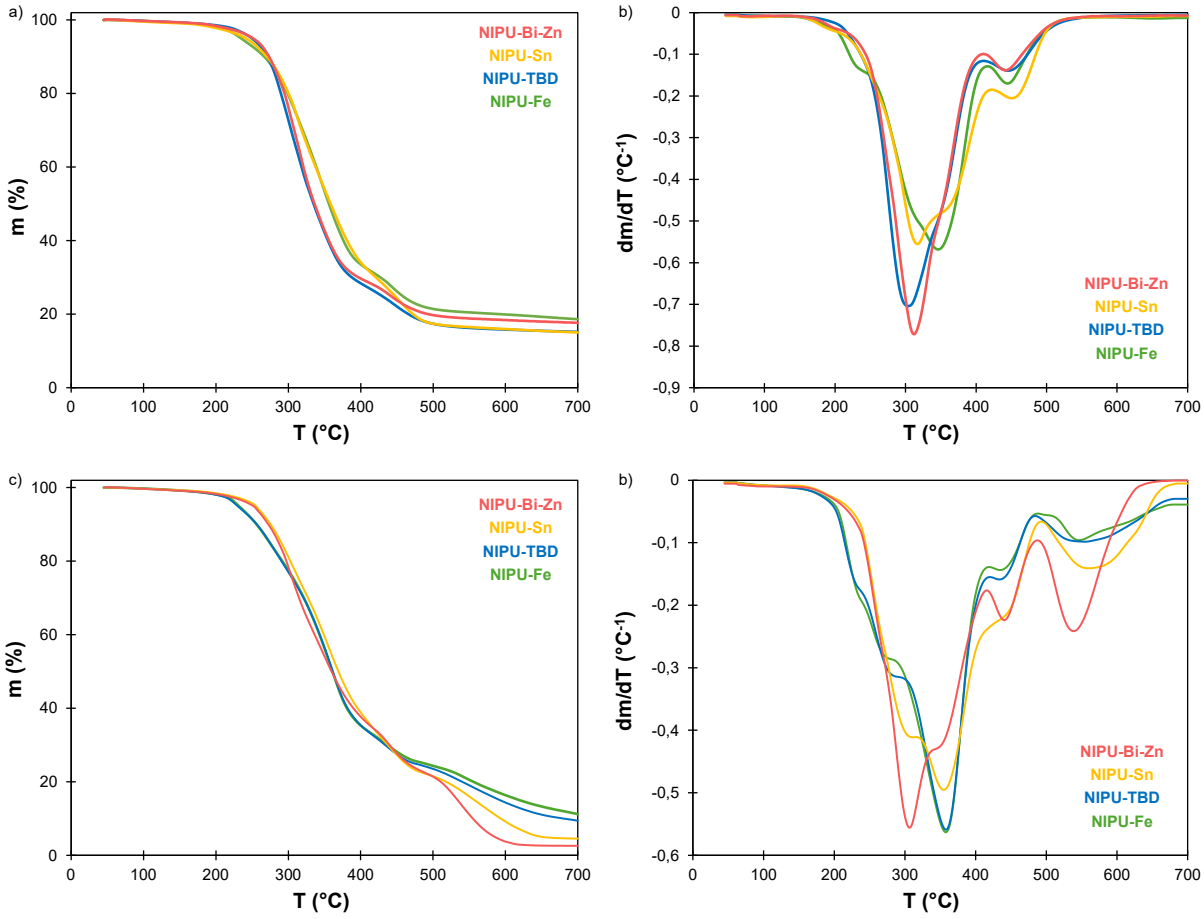

Figure S 13. (a) TGA and (b) DTG curves of the NIPU materials under N_2. (c) TGA and (d) DTG curves of the NIPU materials under air.

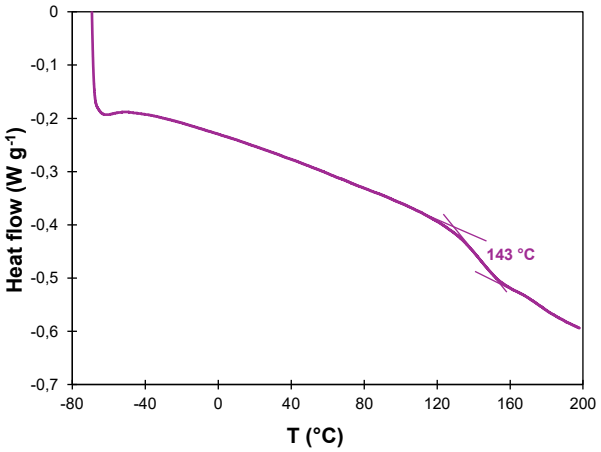

Figure S 14. DSC of SKL.

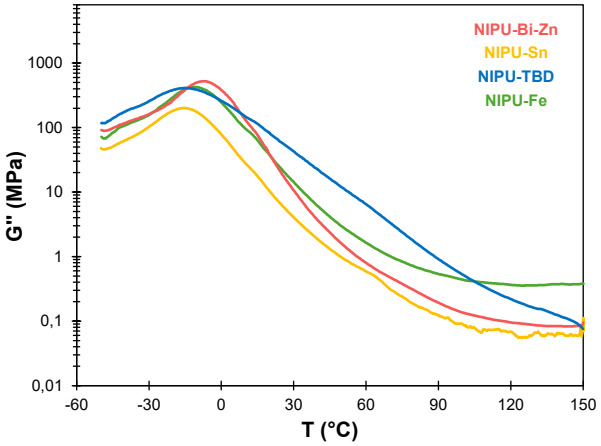

Figure S 15. Loss modulus G'' of the NIPU materials measured by DMA.

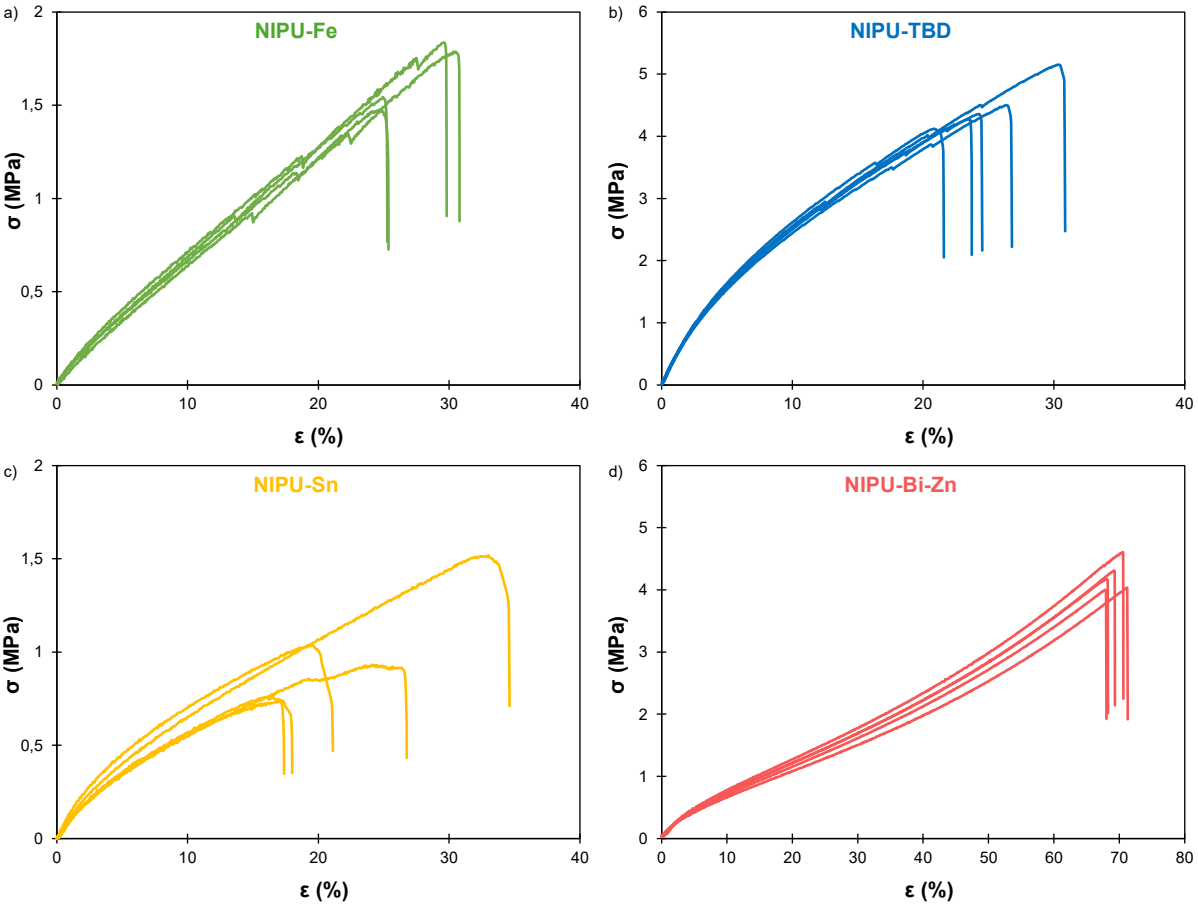

Figure S 16. Stress-strain curves of NIPU materials measured by uniaxial tensile tests: (a) NIPU-Fe, (b) NIPU-TBD, (c) NIPU-Sn and (d) NIPU-Bi-Zn.

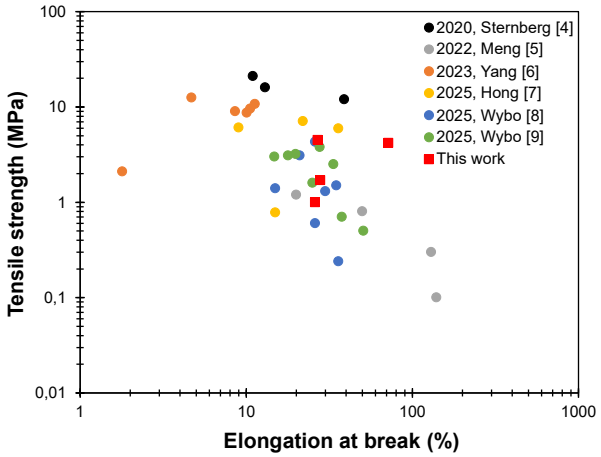

Figure S 17. Comparison of the mechanical properties (uniaxial tensile tests) of the materials prepared in this study with previously reported lignin-based NIPU.[4–9]

Stress relaxation experiments

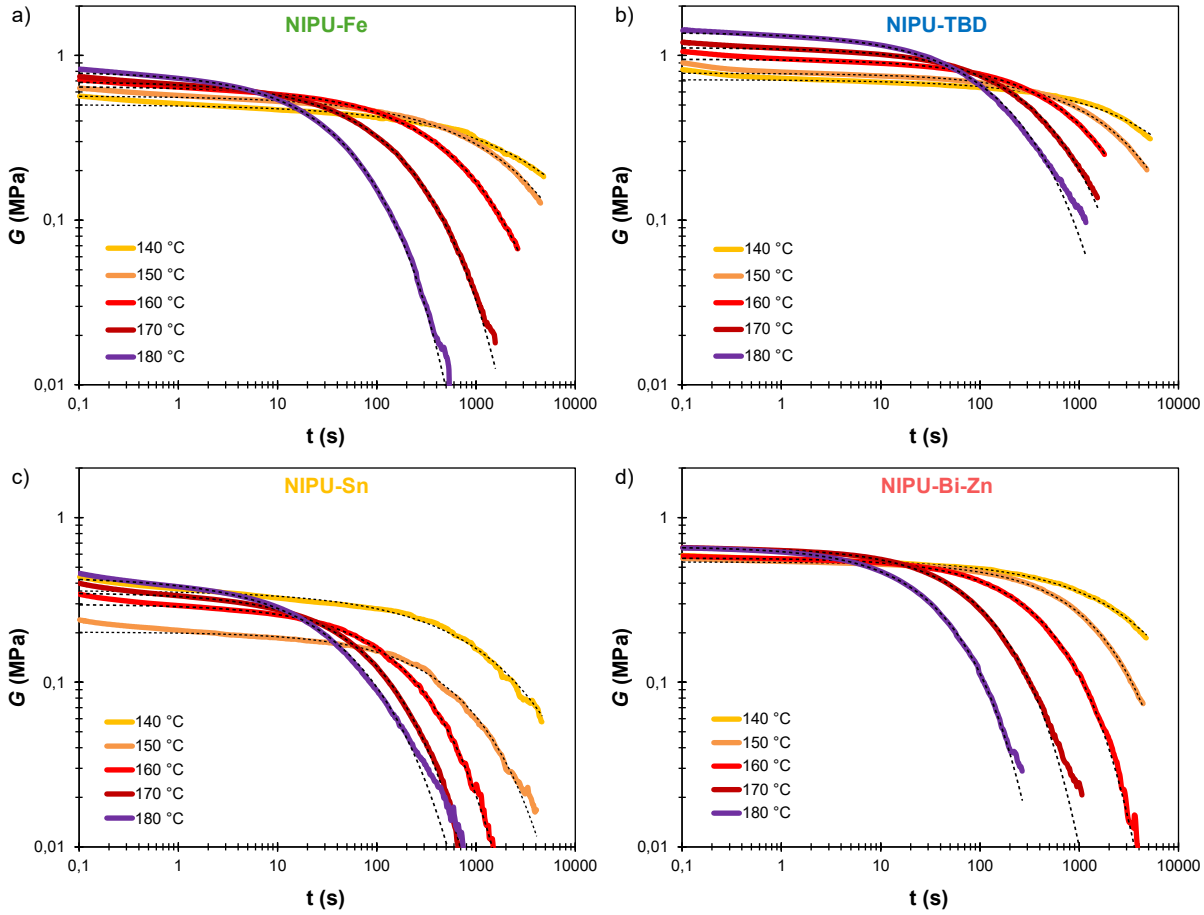

Figure S 18. Stress relaxation of the NIPU materials: (a) ***NIPU-Fe****, (b)* ***NIPU-TBD****, (c)* ***NIPU-Sn*** *and (d)* ***NIPU-Bi-Zn****. The data were fitted with a stretched exponential decay.*

The non-normalized stress relaxation data were fitted with a stretched exponential model (Kohlrausch–Williams–Watts (KWW) function):

$$G\,(t) = G_0\, e^{-(\frac{t}{\tau*})^{\beta}} \qquad \textbf{Equation S1}$$

The fits were performed for t > 1 s. The fit parameters are listed in Tables S1 to S4.

*Table S 1. Results of the fit of stress relaxation data of **NIPU-Fe**.*

T **(°C)**	**τ* (s)**	**β**	G_0 **(MPa)**	R^2	**<τ> (s)**	**ln <τ>**
140	5044	0.45	0.50	> 0.99	12461	9.43
150	2196	0.50	0.57	> 0.99	4426	8.40
160	597	0.56	0.65	> 0.99	996	6.90
170	156	0.60	0.70	> 0.99	233	5.45
180	45	0.62	0.80	> 0.99	65	4.18

*Table S 2. Results of the fit of stress relaxation data of **NIPU-TBD**.*

T **(°C)**	**τ* (s)**	**β**	G_0 **(MPa)**	R^2	**<τ> (s)**	**ln <τ>**
140	8717	0.52	0.71	> 0.99	16153	9.69
150	3053	0.61	0.78	> 0.99	4515	8.42
160	1155	0.63	0.95	> 0.99	1636	7.40
170	428	0.63	1.12	> 0.99	604	6.40
180	169	0.59	1.39	> 0.99	260	5.56

*Table S 3. Results of the fit of stress relaxation data of **NIPU-Sn**.*

T **(°C)**	**τ* (s)**	**β**	G_0 **(MPa)**	R^2	**<τ> (s)**	**ln <τ>**
140	1509	0.50	0.36	> 0.99	2996	8.00
150	764	0.63	0.20	> 0.99	1088	6.99
160	213	0.64	0.30	> 0.99	298	5.70
170	95	0.64	0.35	> 0.99	132	4.88
180	45	0.55	0.44	> 0.99	78	4.35

*Table S 4. Results of the fit of stress relaxation data of **NIPU-Bi-Zn**.*

T **(°C)**	**τ* (s)**	**β**	G_0 **(MPa)**	R^2	**<τ> (s)**	**ln <τ>**
140	4279	0.54	0.56	> 0.99	7540	8.93
150	1606	0.70	0.54	> 0.99	2029	7.62
160	494	0.70	0.57	> 0.99	623	6.43
170	126	0.69	0.66	> 0.99	162	5.09
180	44	0.71	0.67	> 0.99	55	4.01

a) Acid catalyzed transurethanisation (electrophilic or acidic activation)

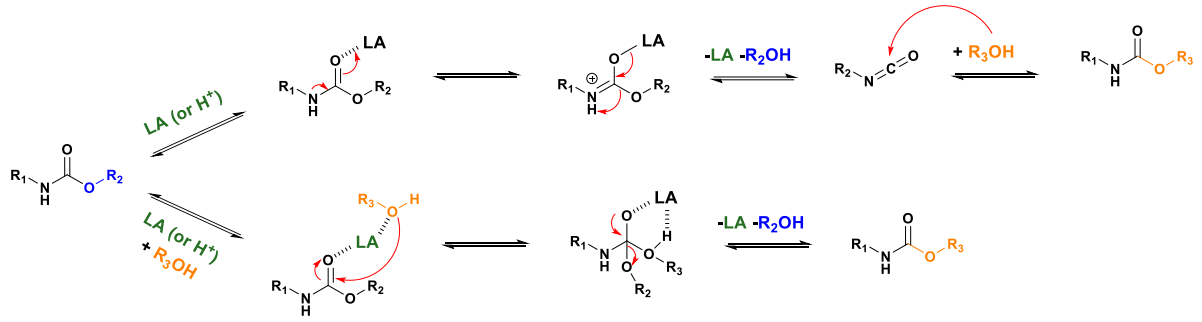

b) Base catalyzed transurethanisation (basic activation)

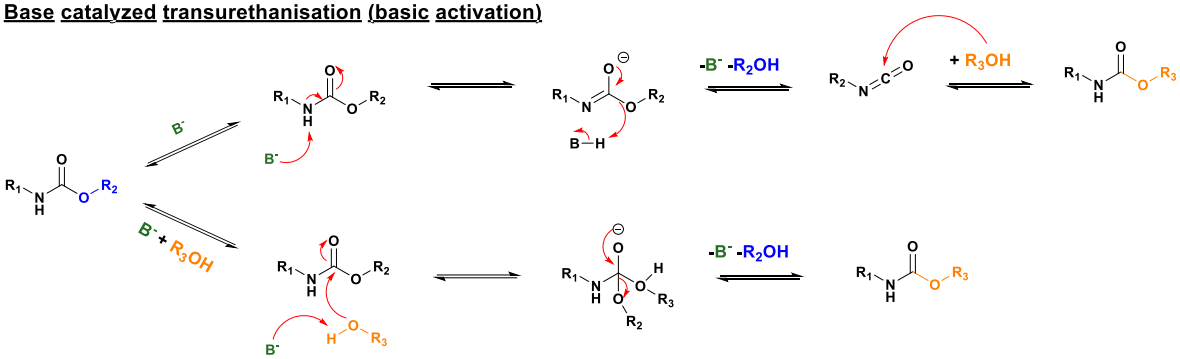

Scheme S 2. Mechanisms of dissociative or associative bond exchange in PU catalysed by (a) acids or (b) bases. Adapted from Bakkali-Hassani et al.[10]

Study of the recyclability of NIPU materials

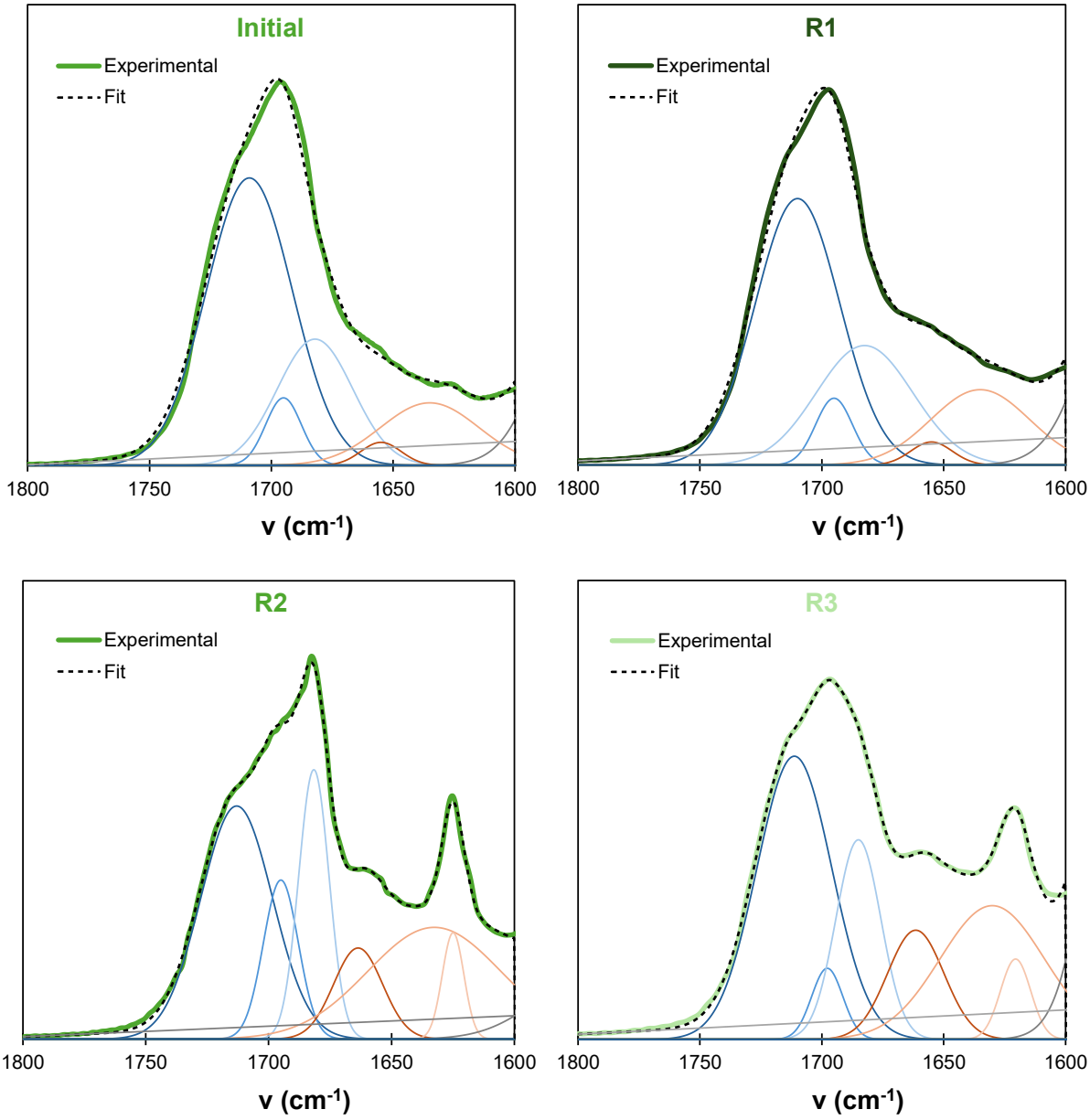

*Figure S 19. Deconvolution of the C=O stretch region of the FTIR spectra of **NIPU-Fe** after each reprocessing cycle. Blue peaks are assigned to urethanes and orange peaks to ureas.*

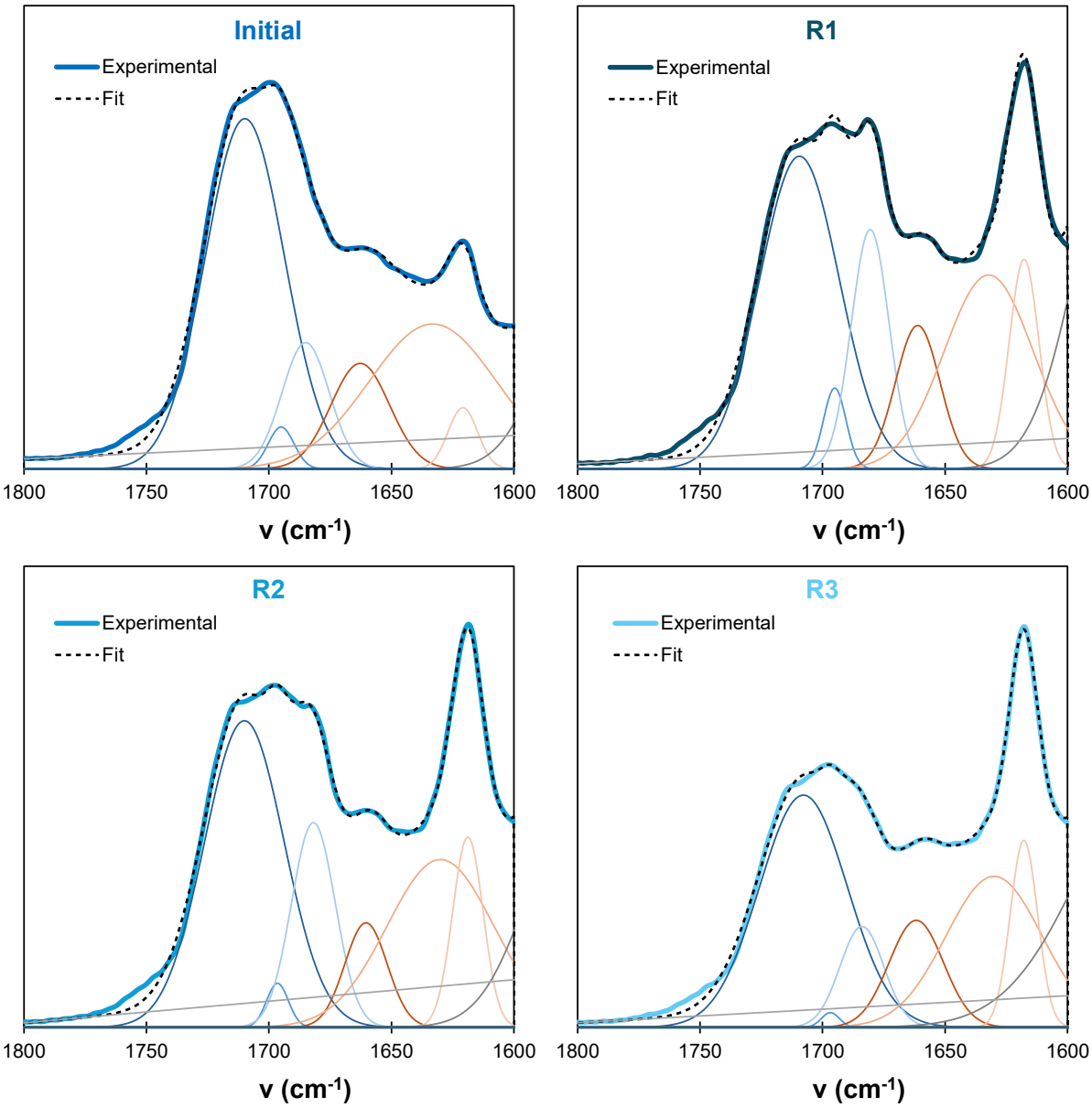

*Figure S 20. Deconvolution of the C=O stretch region of the FTIR spectra of **NIPU-TBD** after each reprocessing cycle. Blue peaks are assigned to urethanes and orange peaks to ureas.*

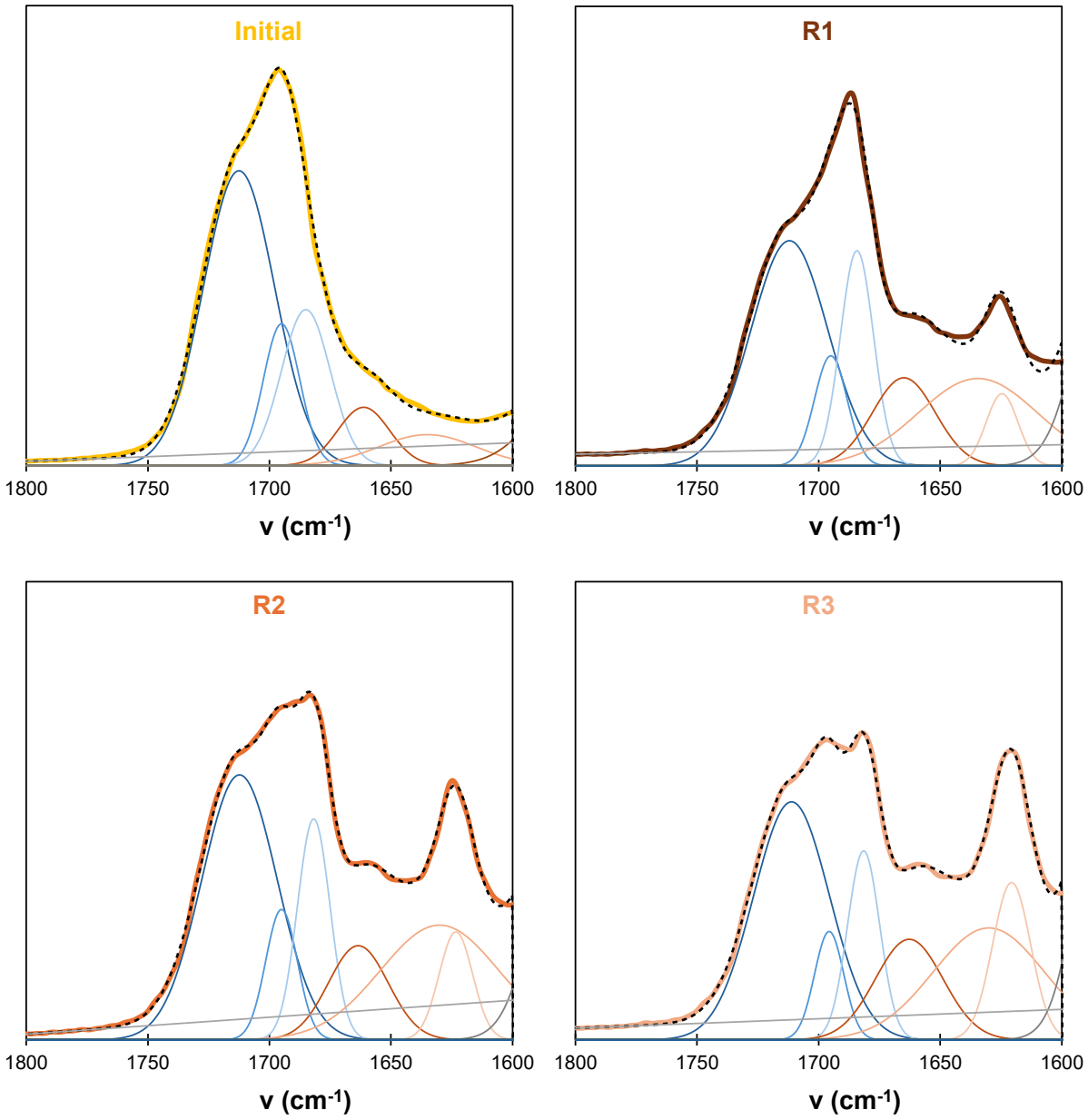

*Figure S 21. Deconvolution of the C=O stretch region of the FTIR spectra of **NIPU-Sn** after each reprocessing cycle. Blue peaks are assigned to urethanes and orange peaks to ureas.*

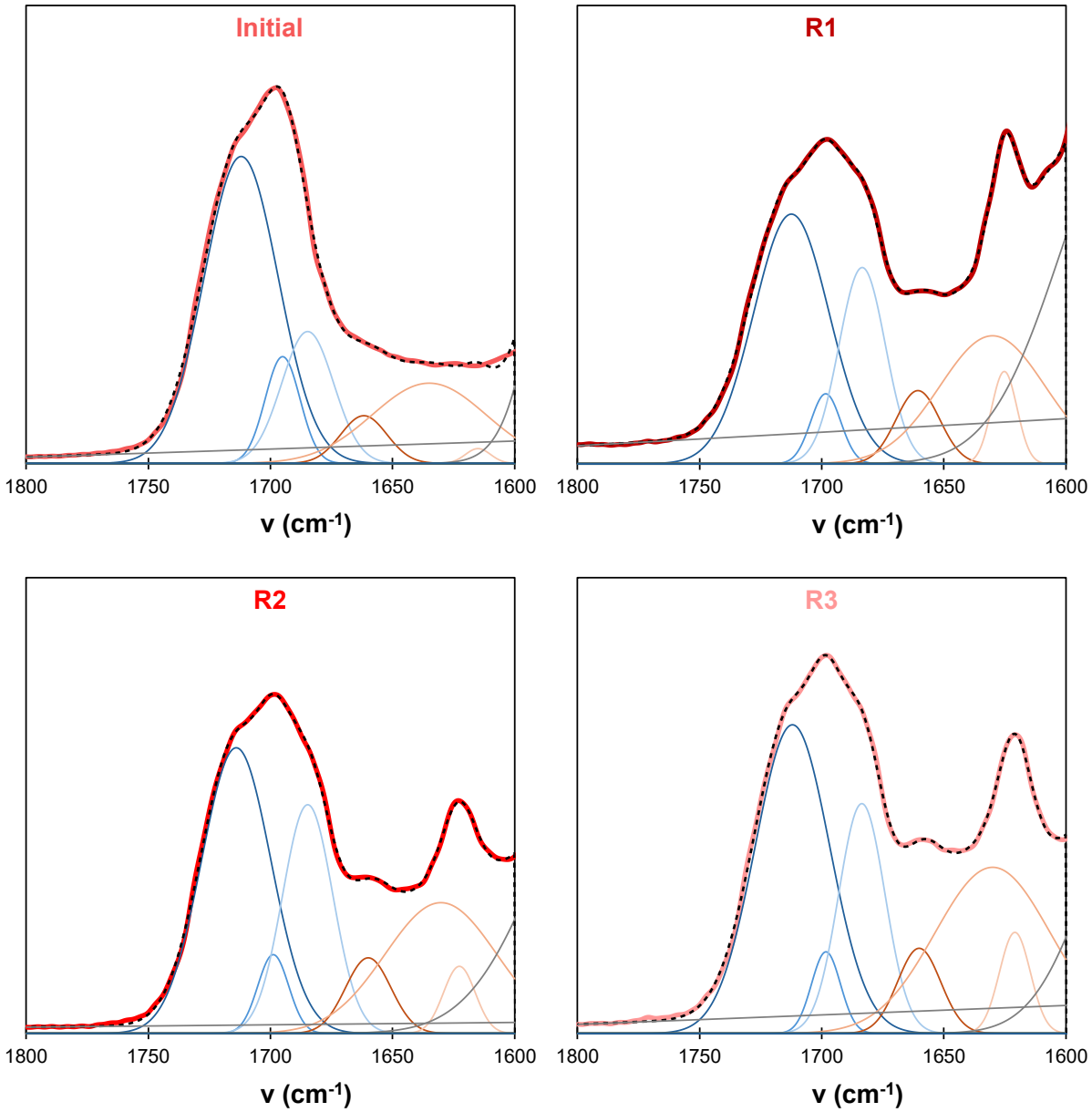

*Figure S 22. Deconvolution of the C=O stretch region of the FTIR spectra of **NIPU-Bi-Zn** after each reprocessing cycle. Blue peaks are assigned to urethanes and orange peaks to ureas.*

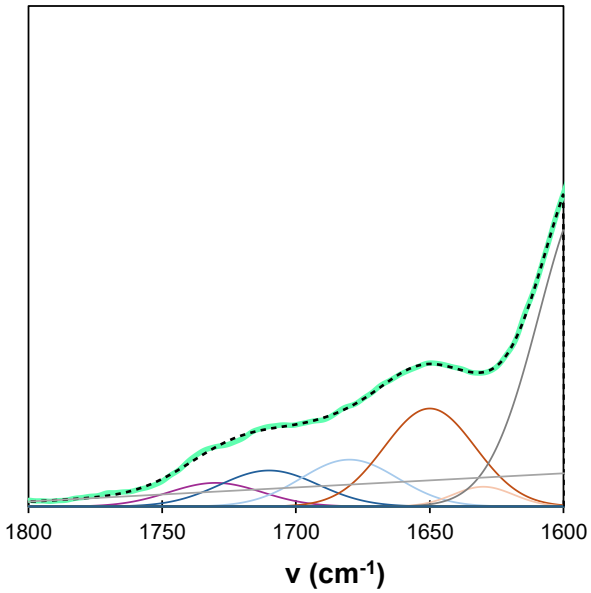

Figure S 23. Detail of the C=O stretch region of the FTIR spectrum of the lignin-based polyol.

Table S 5. Assignments of the peaks used for the deconvolution of the C=O stretch region of the FTIR spectra, according to Jaques et al.[11]

v (cm^{-1})	Assignments
1705 – 1715	Free urethanes
1695 – 1700	Disordered H-bonded urethanes
1680 – 1685	Ordered H-bonded urethanes
1655 – 1665	Free ureas
1630 – 1635	Disordered H-bonded ureas
1615 – 1625	Ordered H-bonded ureas

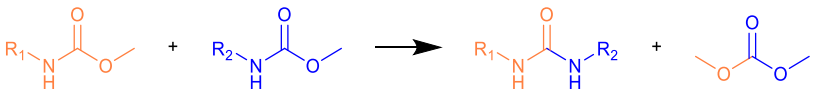

Scheme S 3. Formation of ureas by cross-metathesis reaction of dimethyl carbamates, leading to the release of dimethyl carbonate. Adapted from Kébir et al.[12]

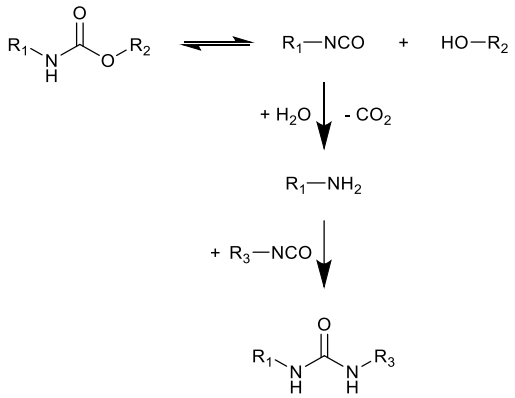

Scheme S 4. Potential mechanism for urea formation during materials reprocessing, involving a dissociative mechanism and the reaction of released isocyanates with residual moisture.

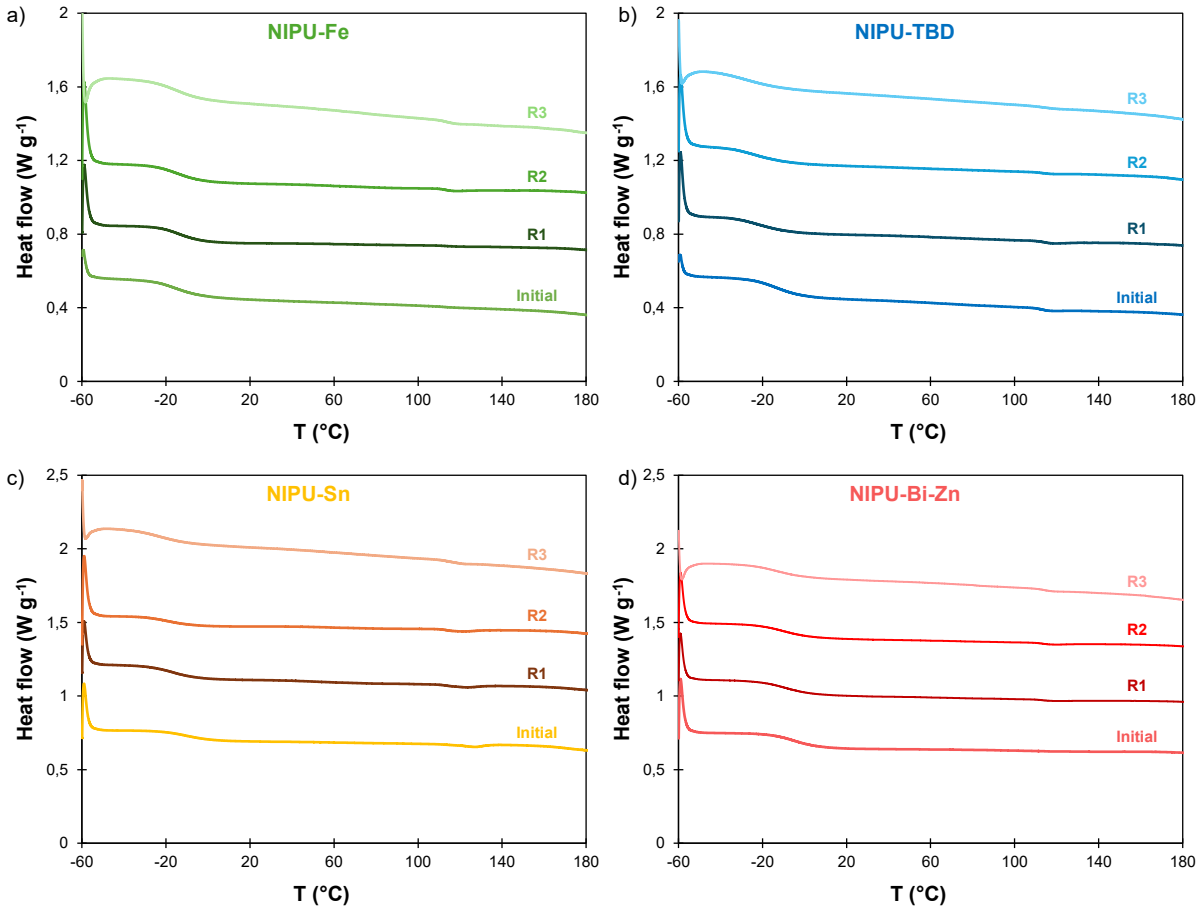

Figure S 24. DSC curves of the NIPU materials after reprocessing: (a) ***NIPU-Fe****, (b)* ***NIPU-TBD****, (c)* ***NIPU-Sn*** *and (d)* ***NIPU-Bi-Zn****.*

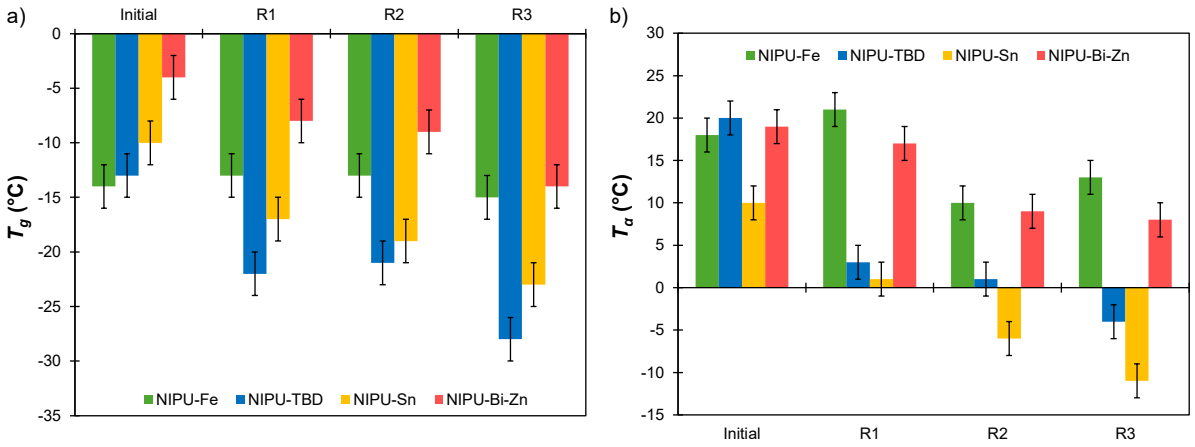

Figure S 25. Evolution of (a) T_g (DSC) and (b) T_α (DMA) of the NIPU materials after reprocessing.

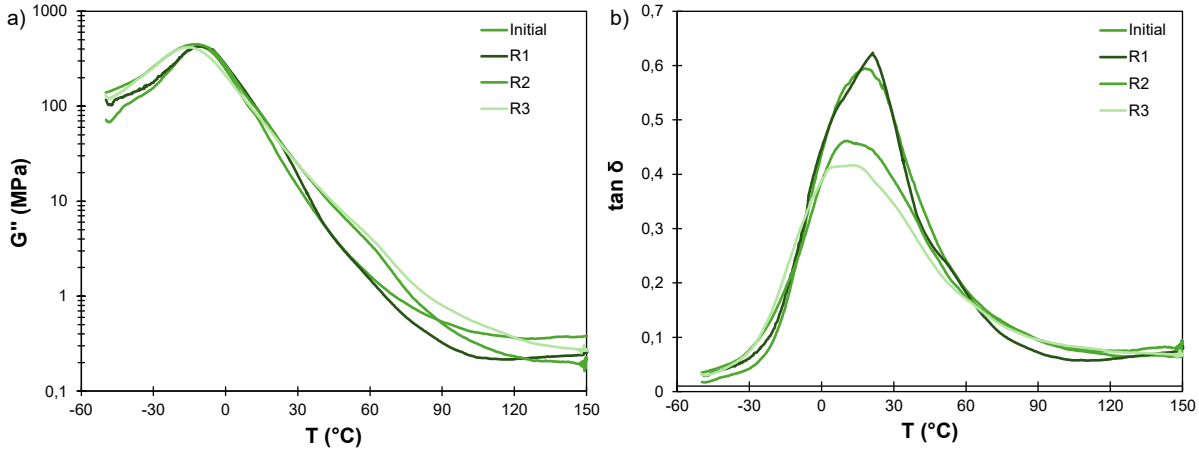

*Figure S 26. DMA curves of **NIPU-Fe** after reprocessing: (a) loss modulus G'' and (b) tan δ.*

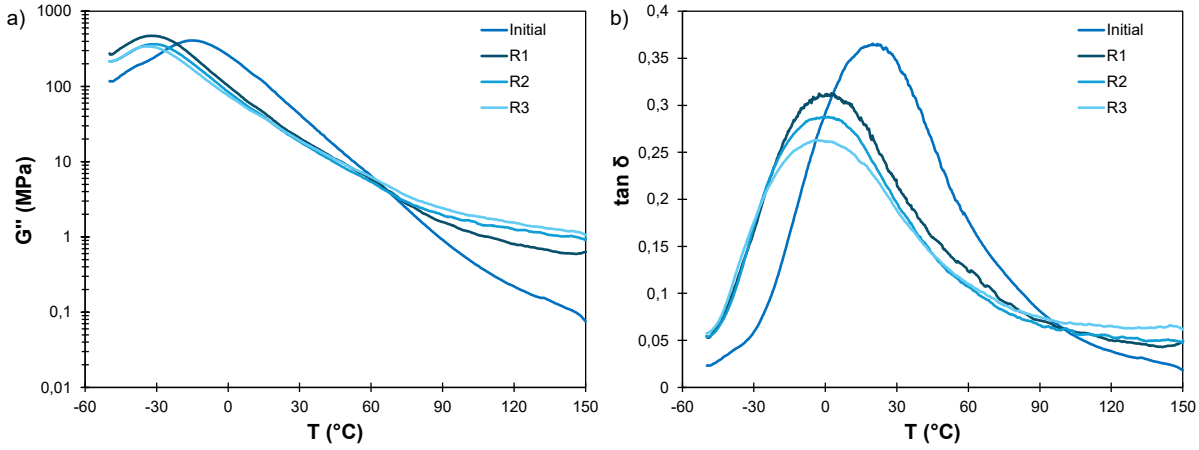

*Figure S 27. DMA curves of **NIPU-TBD** after reprocessing: (a) loss modulus G'' and (b) tan δ.*

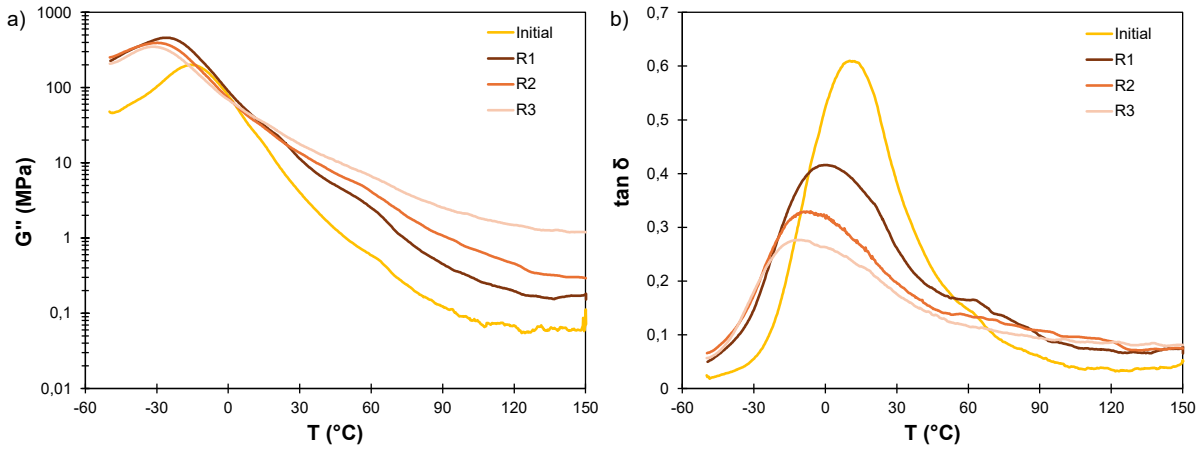

*Figure S 28. DMA curves of **NIPU-Sn** after reprocessing: (a) loss modulus G'' and (b) tan δ.*

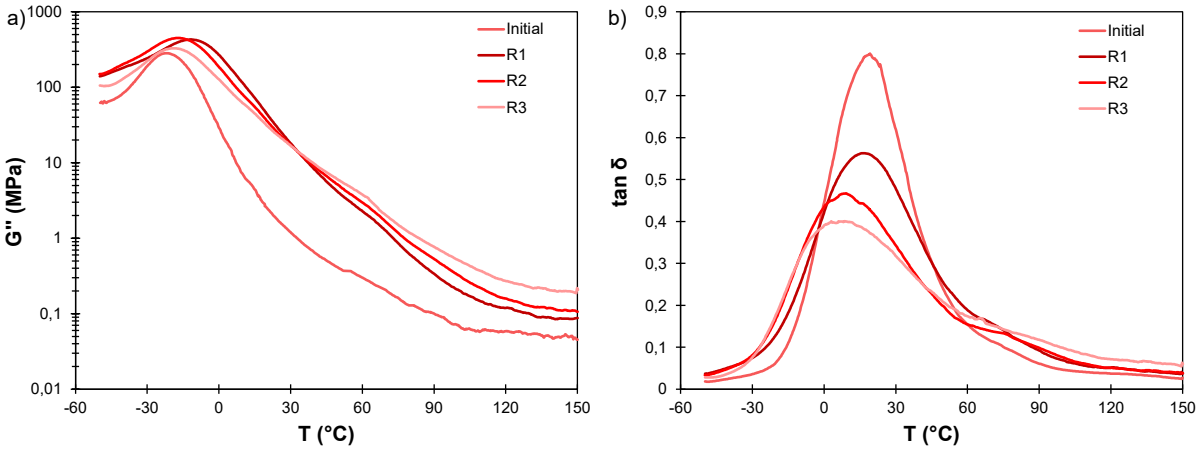

*Figure S 29. DMA curves of **NIPU-Bi-Zn** after reprocessing: (a) loss modulus G'' and (b) tan δ.*

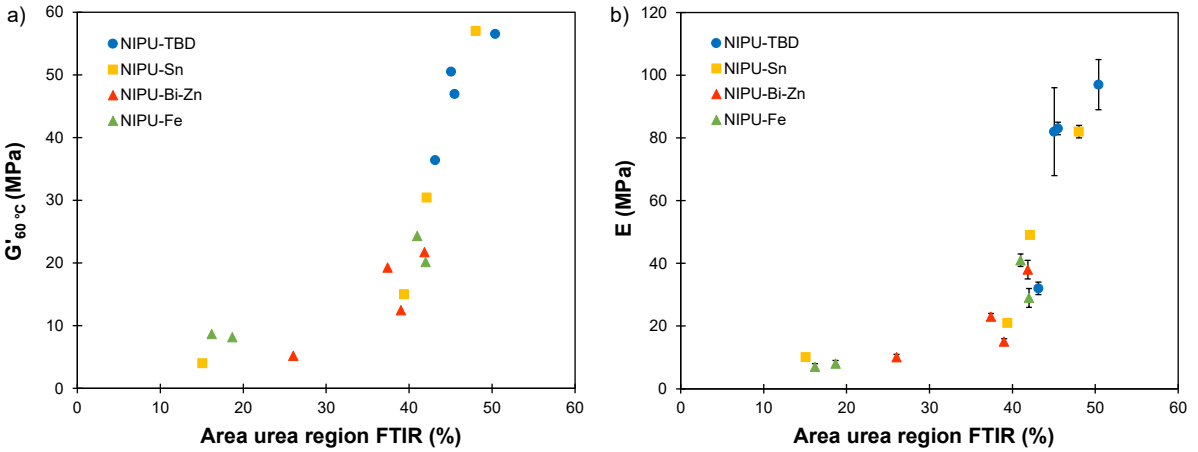

Figure S 30. Correlation between the area of the urea region measured by FTIR and (a) the storage modulus G' at 60 °C measured by DMA and (b) the Young's modulus measured by uniaxial tensile tests.

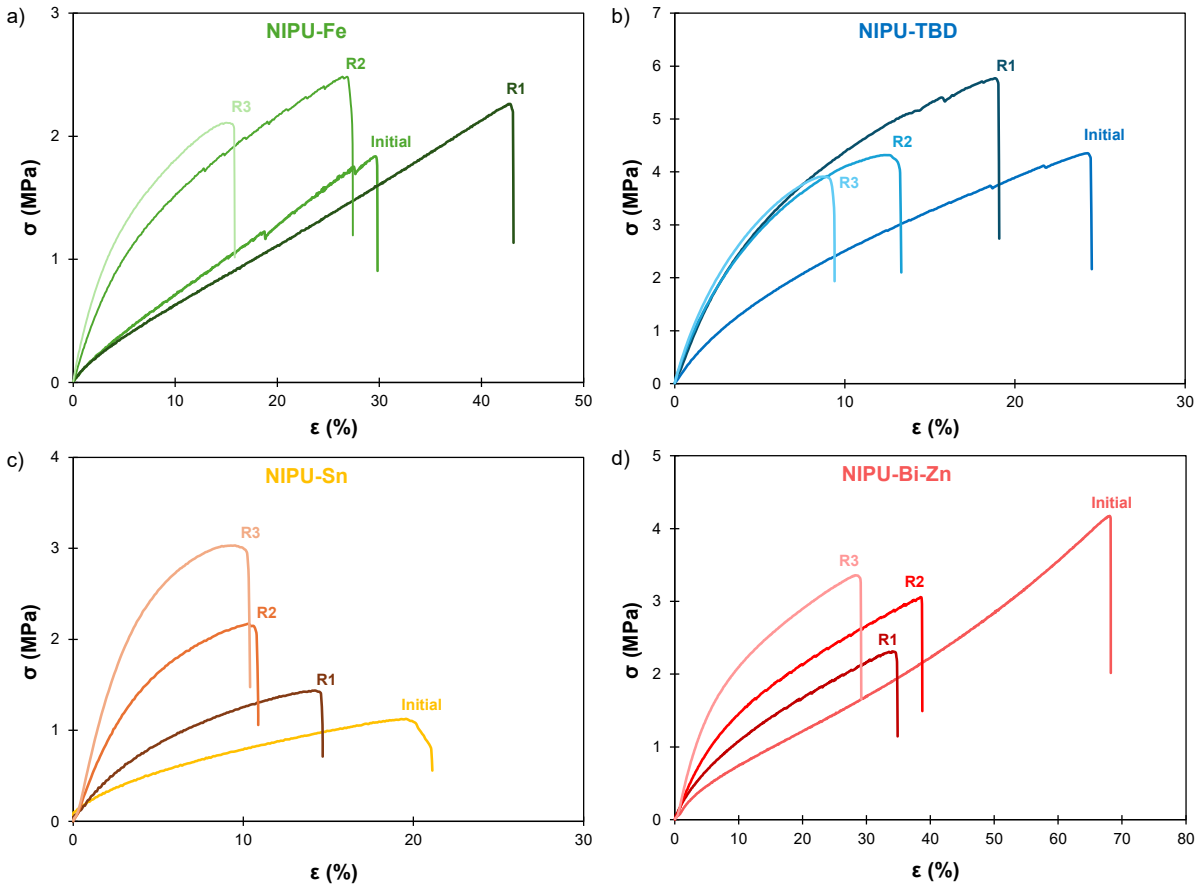

Figure S 31. Uniaxial tensile tests of the NIPU materials after several reprocessing cycles: (a) ***NIPU-Fe****, (b)* ***NIPU-TBD****, (c)* ***NIPU-Sn*** *and (d)* ***NIPU-Bi-Zn****.*

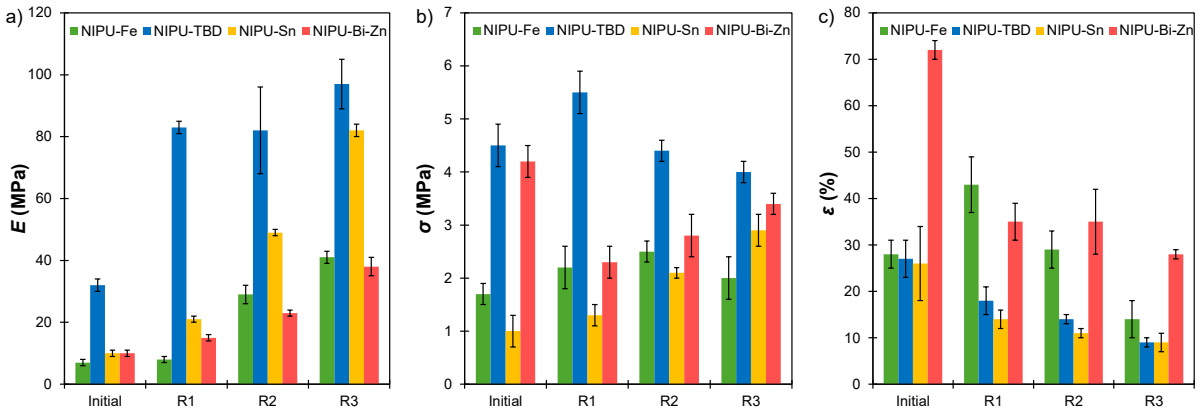

Figure S 32. Evolution of the mechanical properties of the NIPU materials after several reprocessing cycles: (a) Young's modulus, (b) tensile strength and (c) elongation at break.

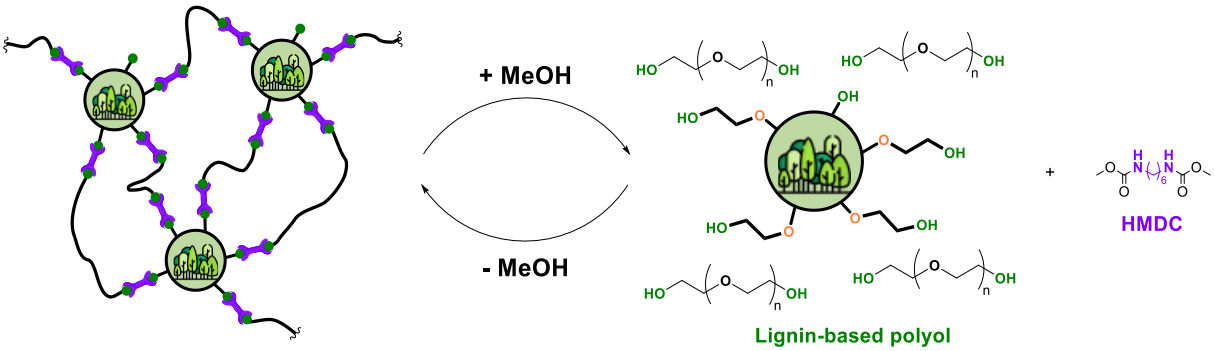

Scheme S 5. Chemical recycling of the NIPU materials by methanolysis.

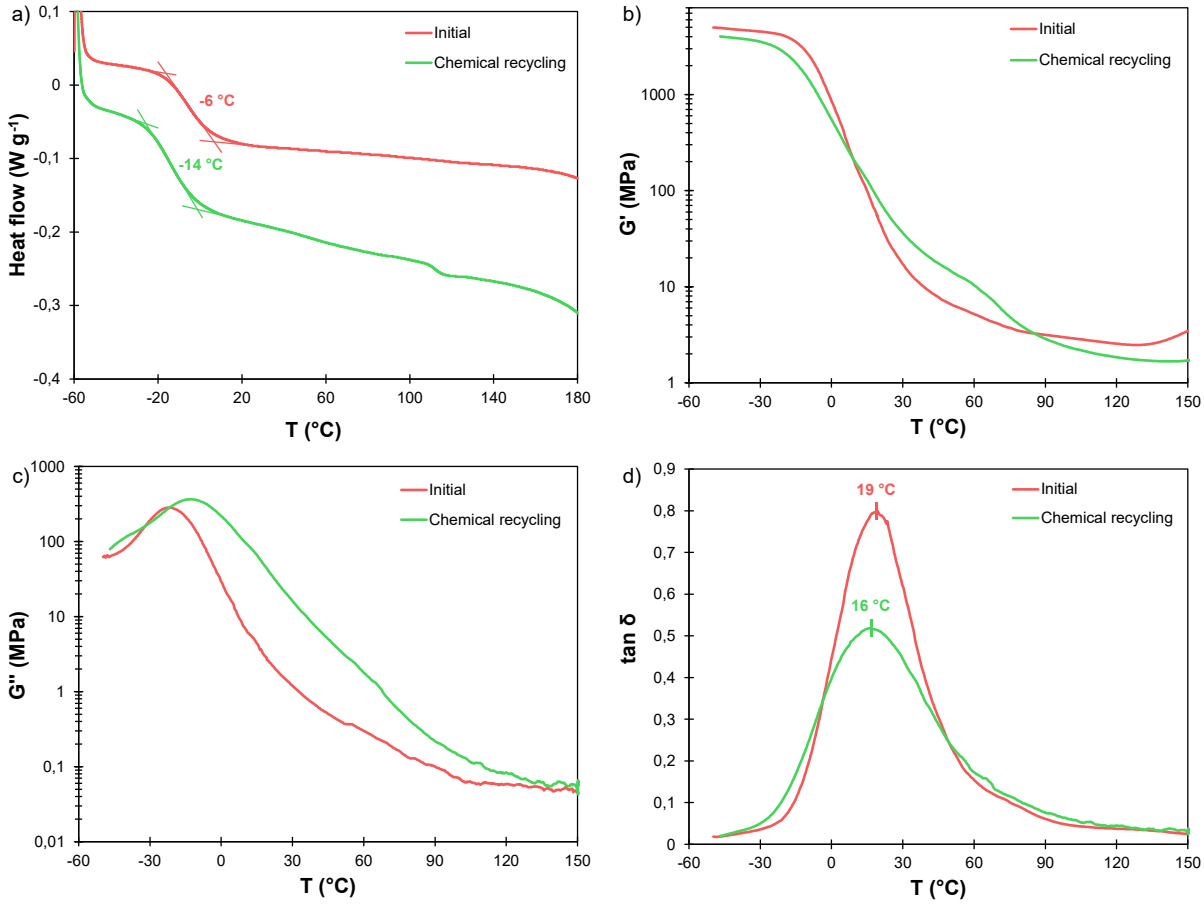

*Figure S 33. Thermal and thermo-mechanical properties of **NIPU-Bi-Zn** after chemical recycling: (a) DSC curves, (b) storage modulus G', (c) loss modulus G'' and (d) tan δ measured by DMA.*

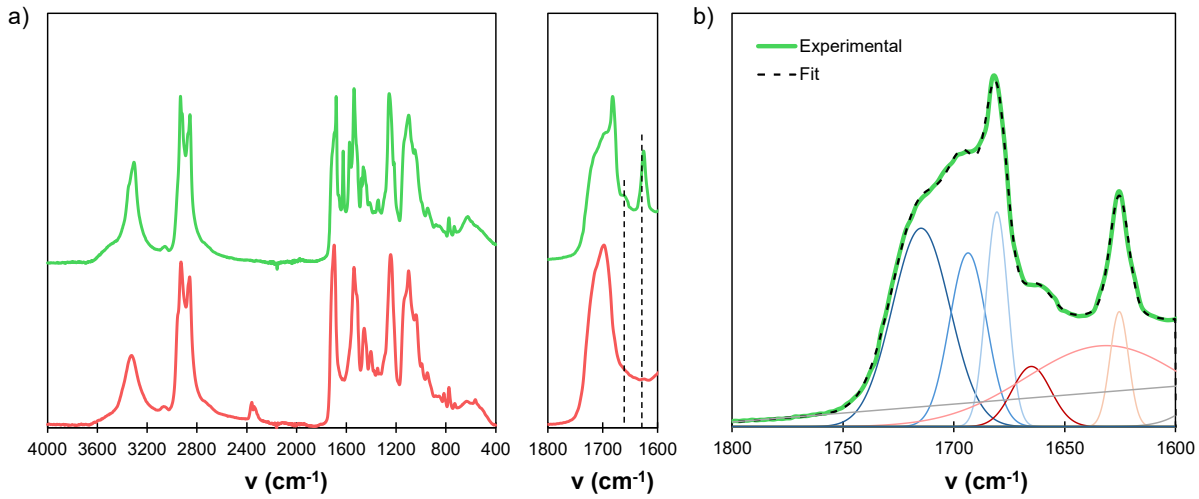

*Figure S 34. (a) FTIR spectra of **NIPU-Bi-Zn** after chemical recycling. (b) Deconvolution of the C=O stretch region of the FTIR spectra of **NIPU-Bi-Zn** after chemical recycling. Blue peaks are assigned to urethanes and orange peaks to ureas.*

References

1 B. Jousseaume, C. Laporte, T. Toupance and J.-M. Bernard, *Tetrahedron Letters*, 2002, **43**, 6305–6307.

2 B. Jousseaume, C. Laporte, T. Toupance and J. M. Bernard, *Tetrahedron Letters*, 2003, **44**, 5983–5985.

3 A. Duval, D. Vidal, A. Sarbu, W. René and L. Avérous, *Materials Today Chemistry*, 2022, **24**, 100793.

4 J. Sternberg and S. Pilla, *Green Chem.*, 2020, **22**, 6922–6935.

5 X. Meng, S. Zhang, B. Scheidemantle, Y. Wang, Y. Pu, C. E. Wyman, C. M. Cai and A. J. Ragauskas, *Industrial Crops and Products*, 2022, **178**, 114579.

6 Y. Yang, H. Cao, R. Liu, Y. Wang, M. Zhu, C. Su, X. Lv, J. Zhao, P. Qin and D. Cai, *Industrial Crops and Products*, 2023, **193**, 116213.

7 H. Hong, Z. Li, H. Wu, D. Wang, L. Liu, W. Luo, T. Yang, K. Yang and J. Yao, *International Journal of Biological Macromolecules*, 2025, **310**, 143259.

8 N. Wybo, A. Duval and L. Avérous, *Materials Today Sustainability*, 2025, **30**, 101117.

9 N. Wybo, E. Cherasse, A. Duval and L. Avérous, *J. Mater. Chem. A*, 2025, **13**, 11557–11572.

10 C. Bakkali-Hassani, D. Berne, V. Ladmiral and S. Caillol, *Macromolecules*, 2022, **55**, 7974–7991.

11 N. G. Jaques, É. Grau, A. Llevot, T. Vidil, M. A. R. Meier and H. Cramail, *Macromolecular Chemistry and Physics*, 2025, **226**, e00207.

12 N. Kébir, M. Benoit and F. Burel, *European Polymer Journal*, 2018, **107**, 155–163.